



# Effect of Concentration Variation on Nickel Cobalt Metal–Organic Framework-Based Electrode Material in Supercapacitor Application

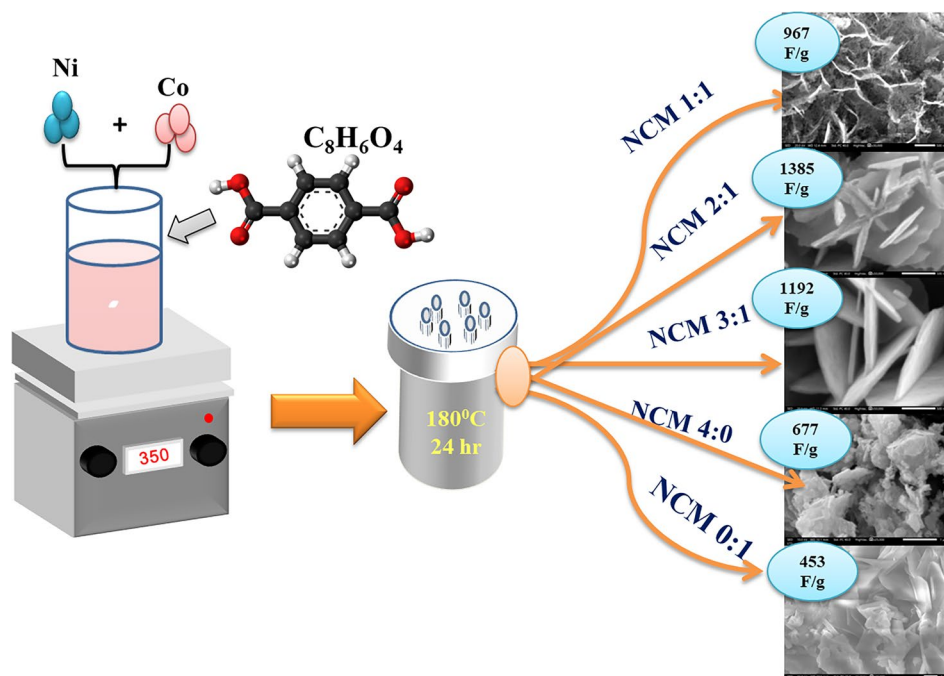
Amruta D. Salunkhe<sup>1,2</sup> · P. K. Pagare<sup>1</sup> · A. P. Torane<sup>1,2</sup>

Received: 3 December 2022 / Accepted: 5 January 2023 / Published online: 13 March 2023  
© The Minerals, Metals & Materials Society 2023

## Abstract

Metal–organic frameworks (MOF) are attracting significant interest as new electrode materials for energy storage applications because of their large specific surface area, porosity, composition, and excellent functionality. Herein, using terephthalic acid as the linker and Ni and Co as the metal centers, a bimetallic metal–organic framework (Ni:Co MOFs = 1:1 2:1 3:1 4:0 0:1) with porous structure was synthesized by the hydrothermal method. The resulting MOFs maintain a flake-like morphology with a high surface area (67.46 m<sup>2</sup>/g), and the pore size of the NCM 2:1 is concentrated to 2–5 nm, which is close to the ideal ion transport channel of electrochemical performance which is suitable for supercapacitor applications. The capacitance of the Ni-Co MOF reached 1385 F/g at 4 mA/cm<sup>2</sup>, and 88.4% capacity was maintained after 3000 cycles, indicating better electrochemical stability. An energy density of 7.8 Wh/kg can be achieved at a power density of 173.07 W/kg and 3.65 Wh/kg is maintained even at a high power density of 692.30 W/kg. These results demonstrate that these Ni-Co MOF bimetallic flakes have great potential as new electrode materials for supercapacitors.

## Graphical Abstract



**Keywords** Ni-Co MOF · supercapacitor · electrode materials · radar plot · hydrothermal method

Extended author information available on the last page of the article

## Introduction

Energy is an integral part of human life. Nowadays, pollution is a central problem due to large populations and also the destruction of natural fuels destroying our environment. Therefore, it is necessary to generate renewable and environmentally friendly energy sources. Electrochemical energy is an indispensable part of clean energy. In many electrochemical energy storage devices, supercapacitors (SC) have become the focal point because of their unique properties such as high specific capacitance, fast charge–discharge rates, and high storage capabilities. The supercapacitor has made its mark in both academics and industries.<sup>1–3</sup> Supercapacitors, also known as electric double-layer capacitors or ultracapacitors, are energy storage devices with outstanding capacity and quiet internal resistance, which are capable of storing and giving energy at moderately large rates as compared to batteries. Execution of supercapacitors depends heavily upon the properties of the material such as electrical conductivity, morphology, chemical stability, and abundant active sites.<sup>4</sup> According to the energy storage mechanism, SC can be divided into two types, an electric double-layer capacitor (EDLC) that stores energy by adsorption/desorption of electrolyte ions, and a pseudo-capacitor in which electrochemical energy is generated from a high-speed redox reaction on the surface. EDLCs mainly use carbon materials such as graphene (Gr), activated carbon, and carbon nanotubes (CNT) as electrode material; on the other hand, pseudo-capacitors mainly use transition metal oxides ( $\text{MnO}_2$ , NiO,  $\text{RuO}_2$ , etc.) and conductive polymers (polyaniline PANI, polypyrrole [PPy], polythiophene [PTh], etc.) are used as electrode materials.<sup>5,6</sup> To further improve the performance of the electrode material, such as specific capacitance and cyclic stability, research on advanced electrode materials with porous structure, large specific surface area, numerous electrically active sites, and conductivity has become the focus of research on high-performance supercapacitors.<sup>7</sup>

Metal–organic frameworks (MOFs) are crystalline solids including indefinite lattices constructed from inorganic secondary installation components and organic linkers, connected by coordination bonds of intermediate vitality. MOFs are very different materials from others because they have large size, good porosity, pore size, shape, dimensionality, and chemical environment that can be best adapted.<sup>8,9</sup> Presently, MOFs have been used as gas storage and separators,<sup>10</sup> supercapacitors,<sup>11</sup> heterogeneous catalysts,<sup>12</sup> biomedicine,<sup>13</sup> chemical sensors,<sup>14</sup> and proton conductivity.<sup>15</sup> Attention to this new type of porous material is rapidly increasing, as it has potential application in many fields. However, composites of MOFs have also been used in the field of electrochemical

energy storage, such as in supercapacitors, lithium-ion batteries, and fuel cells.<sup>16</sup> Still, MOFs are crystalline in nature because their ordered networks build up through coordination bonds among ligands and the metal center. The structure of MOFs is adaptable and the electrical conductivity is commonly insufficient for carbon-based electrode materials.<sup>17</sup> To date, MOF-based electrode materials can be broadly classified into two categories. In some cases, MOF was used as a sacrificial template for the preparation of MOF-derived materials due to its large surface area, tunable small pore size, and efficient contact between electrodes and electrolytes.<sup>18</sup> Meanwhile, due to the low electrical conductivity of the derived materials and to improve the performance of the materials, many composites based on porous carbons derived from MOF or based on metal oxides derived from MOFs have been studied.<sup>19</sup> Accordingly, MOFs and metal hydroxide composites with high stability and good conductivity are very quick in the construction of supercapacitor electrodes.<sup>20</sup> In specific, porous transition metal hydroxide nanoparticles synthesized from MOFs can demonstrate several morphologies, such as a spherical, dodecahedral, cubic, and tubular, and their particle sizes range from 10 nm to 100 nm.<sup>21–25</sup> Various types of MOF-based electrode materials are available in electrochemical applications. Among them, nickel cobalt-derived MOFs are considered promising electrode materials for supercapacitors due to their high theoretical capacitance, easy synthesis, and environmental friendliness. Therefore, sizeable efforts are made to attain high-performance Ni-Co MOF electrode materials.<sup>26,27</sup> The Ni-MOF material has a large surface area and porous structure; hence, it shows amazing electrochemical properties. For example, Du et al.<sup>28</sup> synthesized a two-dimensional nickel-based metal–organic framework which shows a higher specific capacitance of 1057 F/g at 1 A/g and stability is 70% after 2500 cycles. Gao et al.<sup>29</sup> reported the synthesis of Ni-MOF which has a specific capacitance of 804 F/g using the hydrothermal method. Because of its low electrical conductivity and poor structural stability, nickel-based MOFs are not used in electrochemical energy storage devices. In the case of cobalt MOF, Xuan et al.<sup>30</sup> synthesized a Co-MOF at different temperatures through the solvothermal method and reported a specific capacitance of 952.5 F/g synthesized at 150°C at a current density of 0.25 A/g, demonstrating excellent stability and electrical conductivity. Lee et al.<sup>31</sup> reported the synthesis of Co-based MOF material which has specific capacitance of 206.76 F/g and high stability after 1000 cycles and only a loss of 1.5% in capacitance for an electrochemical test. Cobalt-based MOF has higher cyclic stability but poor specific capacitance.<sup>32</sup> Improvement is required in monometallic electrical conductivity,

stability, and specific capacitance. Various types of bimetallic–organic frameworks show unique capacitive performance. Wang et al.<sup>33</sup> reported a bimetallic Ni-Co MOF flower-like structure that exhibited a high specific capacitance of 1300 F/g at 1 A/g with a higher stability 1070 F/g at 10 A/g. After a number of cycles, conductivity is enhanced because Ni<sup>2+</sup> and Co<sup>2+</sup> ions interact to produce a synergistic effect. Sriekesh et al.<sup>34</sup> reported that cobalt concentration strongly affected nickel-based MOF. At low concentrations of cobalt, it has higher specific capacitance. In addition, Gholipour et al.<sup>35</sup> reported that Ni-Co-based bimetallic MOF has excellent specific capacitance of 1049 F/g at 1 A/g with high stability of 97.4% after 5000 cycles. Overall, studies on the direct use of monometallic MOFs are rare due to their low conductivity, high steric hindrance, and inadequate electrolytes. Therefore, it is desirable to produce bimetallic MOFs with a multidimensional structure, improved conductivity, reduced steric hindrance, and good compatibility with electrolytes. In this study, Ni-Co MOF with a flake-like structure was synthesized by the hydrothermal synthesis method. The novelty of our work lies in increasing the nickel concentration which results in a more open hierarchical flake-like structure that facilitates contact between the active site and electrolyte ions. Also, in Ni-Co MOF, some Co<sup>2+</sup> is replaced by Ni<sup>2+</sup>, creating more empty holes and improving the conductivity of the MOF material.<sup>33</sup> By using the strategy of increasing nickel content, not only are chemical costs reduced, but the conductivity of MOF material is also improved. On the other hand, the improved oxidation state and synergies of bimetals in MOFs are beneficial in improving electrochemical performance. The novelty also lies in comparison of the morphology for the bimetallic MOF synthesized without the structure-directing agents. In addition, Ni-Co MOF electrode material has been assembled that exhibits excellent energy and power densities. These advantages and the synergistic effect between Ni and Co enhance the electrochemical activity of Ni-Co MOF, thus obtaining the best specific capacitance from 1385 F/g at 4 mA/cm<sup>2</sup> in 1 M KOH.

## Experimental

### Materials

Nickel nitrate hexahydrate (Ni(NO<sub>3</sub>)<sub>2</sub>·6H<sub>2</sub>O) 99% pure, cobalt (II) nitrate hexahydrate (Co(NO<sub>3</sub>)<sub>2</sub>·6H<sub>2</sub>O) 98% pure, *N,N*-dimethylformamide (DMF), terephthalic acid (C<sub>8</sub>H<sub>6</sub>O<sub>4</sub>) 98% pure, ethanol, and hydrochloric acid 35%

extra pure AR grade chemicals were used to prepare Ni-Co MOF material.

### Synthesis of Ni-Co MOFs

In the present work, Ni-Co MOF material is synthesized by the hydrothermal method. Nickel nitrate hexahydrate (Ni(NO<sub>3</sub>)<sub>2</sub>·6H<sub>2</sub>O) and cobalt (II) nitrate hexahydrate (Co(NO<sub>3</sub>)<sub>2</sub>·6H<sub>2</sub>O) were used as the starting materials, terephthalic acid (C<sub>8</sub>H<sub>6</sub>O<sub>4</sub>) was used as the organic linker and a mixture of ethanol, DMF and double distilled water (DDW) was used as a solvent. A solution of 0.1 M Ni(NO<sub>3</sub>)<sub>2</sub>·6H<sub>2</sub>O and 0.1 M Co(NO<sub>3</sub>)<sub>2</sub>·6H<sub>2</sub>O in 30 mL DDW was added to another solution of 0.05 M terephthalic acid dissolved in 30 mL of ethanol and 30 mL of DMF. After that, the prepared solution was stirred by magnetic stirring for 60 min to obtain a clear, homogeneous solution. Then the solution was transferred into a 150 mL Teflon-lined autoclave. The autoclave was maintained at 180°C for 24 h. After that, the autoclave was left to cool naturally to room temperature. The resulting material precipitate was washed several times with ethanol. The resultant product was dried overnight in a vacuum oven at 80°C. The resultant pink powder was denoted as Ni-Co MOF. The effect of concentration on nickel and cobalt content was studied by varying the ratio between them. Herein, the molar ratio of nickel and cobalt varied as 1:1, 2:1, 3:1, 4:0, 0:1 (Ni:Co) and was denoted as NCM 1:1, NCM 2:1, NCM 3:1 NCM 4:0 and NCM 0:1 as seen in Fig. 1.

### Preparation of the Working Electrode

Ni foam was used as a current collector. Prior to showing supercapacitor properties, working electrodes were prepared using Ni-Co MOF material (80%), acetylene black (10%) and polyvinylidene fluoride (PVDF) (10%) in *N*-methyl-2-pyrrolidinone (NMP). The resultant slurry was coated onto nickel foam (1 cm<sup>2</sup>) and dried overnight at 80°C. The electrodes prepared from the NCM 1:1, NCM 2:1, NCM 3:1, NCM 4:0 and NCM 0:1 powder were used for electrochemical performance testing. The mass loading of active material is approximately 10 mg/cm<sup>2</sup>.

### Characterizations of Ni-Co MOF

The crystalline nature and phase confirmation of Ni-Co MOF material were characterized by XRD using a Bruker D<sub>2</sub> phaser instrument with Cu-K $\alpha$  radiation (wavelength = 1.5406 Å). Morphological study of synthesized material was carried out by SEM using a JEOL JSM-IT200 instrument. The functional group and mode of vibrations were studied using Raman and FT-IR spectroscopy, and elemental mapping of the material was observed by EDS.

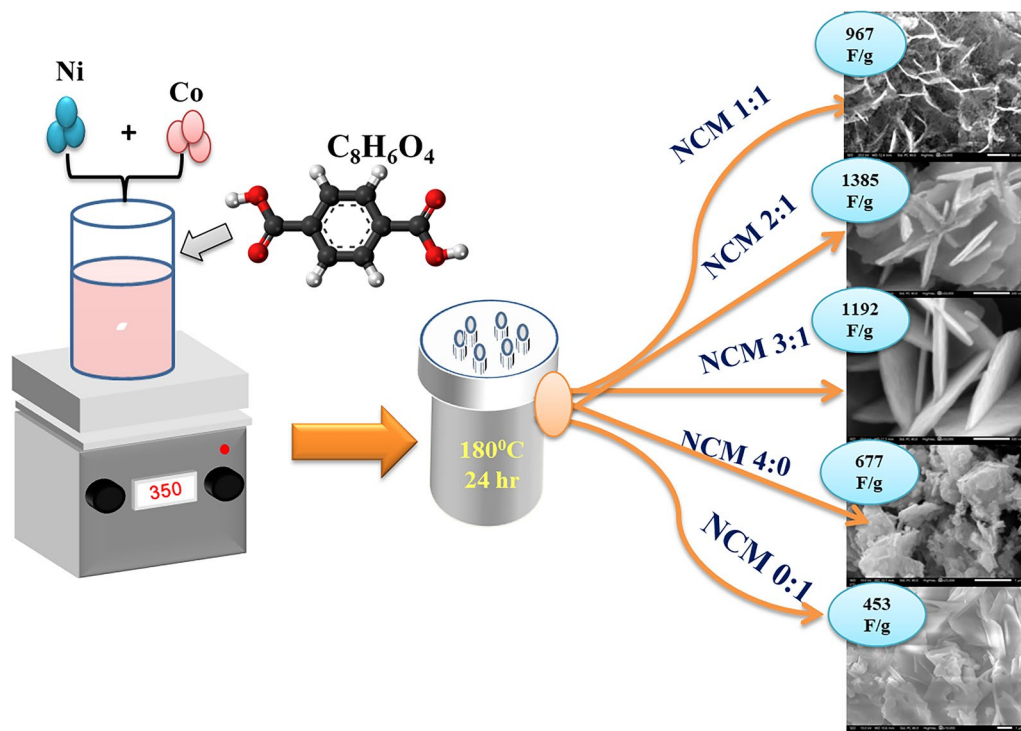


**Fig. 1** Schematic illustration of the preparation of Ni-Co MOF material.

Brunauer–Emmett–Teller (BET) analysis was used for the evaluation of the surface area and pore size distribution by using N<sub>2</sub> adsorption–desorption isotherms. Electrochemical properties of the NCM electrodes were studied by cyclic voltammetry (CV), galvanostatic charge–discharge (GCD), and electrochemical impedance spectroscopy (EIS) on an electrochemical workstation.

### Electrochemical Measurements

The effect of different concentrations on the electrochemical performance of Ni-Co MOF was studied with the help of a three-electrode system. For this study, silver chloride (Ag/AgCl) was used as the reference electrode and platinum wire as the counter electrode. For electrochemical measurements, a potential window range of 0–0.8 V and scan rate from 5 to 100 mV/s were used to test the performance in nickel cobalt metal–organic framework electrodes. Electrochemical testing of synthesized material was carried out using a 1.0 M KOH electrolyte system. The 1 cm<sup>2</sup> area of the working electrode is embedded in the electrolyte for precise electrochemical measurements. The specific capacitance of the material is given by

$$C_s = \frac{\int idV}{ms\Delta V} \quad (1)$$

The energy density and power density are calculated using Eqs. 2 and 3, respectively.

$$ED = \frac{C_p \times (\Delta v)^2}{2 \times 3.6} \quad (2)$$

$$PD = \frac{3600 \times E_g}{\Delta t} \quad (3)$$

where  $\Delta v$  voltage window of three electrode and  $i$  is the discharge current. The CV curves at different scan rates and peak potentials give the charge storage behavior in nickel cobalt metal–organic framework.<sup>36,37</sup>

## Results and Discussion

### Structure and Morphology Characterization

When growing nanomaterial using hydrothermal methods, the reaction temperature plays an important role by changing the basic properties of the nanomaterial, such as crystallinity, surface morphology, surface energy, pore structure, and

corresponding electrochemical performance. With sufficient porosity and a uniform layered structure, active materials are excellent as electrodes for SCs because they facilitate the path of electrolyte ions during electrochemical reactions and help improve energy storage capacity. Here, a series of Ni-Co MOFs with the same reaction conditions except for the reaction concentration was prepared as electrode material through a one-step hydrothermal method. To achieve the highest electrochemical performance, it is very necessary to control the morphology of the as active material, especially its size and shape, by optimizing preparation conditions such as temperature and reaction time. In this case, flake-like Ni-Co MOF have been prepared active material via the hydrothermal method in which an organic linker ( $C_8H_6O_4$ ) and metal precursors Ni ( $Ni(NO_3)_2 \cdot 6H_2O$ ) and Co ( $Co(NO_3)_2 \cdot 6H_2O$ ) were used in a non-aqueous system. As seen in the schematics, the morphology of the Ni-Co-MOFs changes with change in reaction concentration, leading to changes in electrochemical performance.

The XRD structures of Ni-Co MOFs were compared with their respective concentration changes to study the formation of Ni-Co MOFs, and their respective concentration comparisons for NCM 1:1, NCM 2:1, NCM 3:1 and NCM 4:0 are shown in Fig. 2a, respectively. The organic binder coordinates strongly with nickel and cobalt ions to form a new crystal structure in Ni-Co MOF. And the diffraction patterns simulated from the single crystal data of  $[Ni_3(OH)_2(C_8H_6O_4)_2(H_2O)_4] \cdot 2H_2O$  (CCDC-985792) and  $[Co_2(OH)_2C_8H_6O_4]$  (CCDC 153,067)<sup>38</sup> which directly confirms that the Ni-Co MOF has a MOF structure. The XRD patterns of the MOFs show the presence of sharp and narrow peaks, indicating the highly crystalline nature of Ni-Co MOFs. According to the x-ray pattern, the samples show similar diffraction peaks, but the intensity of those peaks slightly increases as the concentration of nickel ions increases. This shows that although NCM 4:0 does not break the bond between the metal center and the organic

linker, the intensity of the diffraction peak characteristic of NCM 1:1 is reduced due to the poor electrostatic interaction between the Co ion and the organic linker.<sup>39</sup> The crystal size of Ni-Co MOF was determined at 36.16, 43.93, 55.79 and 28 nm for NCM 1:1, NCM 2:1, NCM 3:1 and NCM 4:0, respectively, giving a high intensity peak possible is calculated using a famous Debye Scherrer formula for the Eq. 4.

$$D = \frac{0.9\lambda}{\beta \cos\theta} \quad (4)$$

where  $D$  is the crystalline size,  $\theta$  is the Bragg diffraction angle of the diffraction peaks,  $\lambda$  is the wavelength and  $\beta$  is the full width at half maxima of the peak. The crystallite size directly affects the electrochemical performance of Ni-Co MOF.<sup>40</sup> The shifting of the major peak from the angle of  $11.32^\circ$ – $12.81^\circ$  with an increase in nickel content confirms that compositions of NCM 1:1, NCM 2:1, NCM 3:1, and NCM 4:0 are nickel cobalt metal–organic frameworks. Similar results of peak shifting in the XRD pattern by the addition of atoms in the formation of binary material were observed by Li et al.<sup>41</sup> This phenomenon is due to the partial replacement of some Co atoms by Ni atoms during product formation. The observed shift is due to the incorporation of Ni and Co atoms during the formation of the material.

**Table 1** Comparison of crystallite size and interplanar spacing from NCM sample

Samples	$2\theta$	Crystallite size ( $D$ , nm)	Interplanar spacing ( $d$ )
NCM 1:1	11.32	36.16	6.9 Å
NCM 2:1	11.72	43	7.2 Å
NCM 3:1	12.29	55.79	7.6 Å
NCM 4:0	12.81	28	7.8 Å

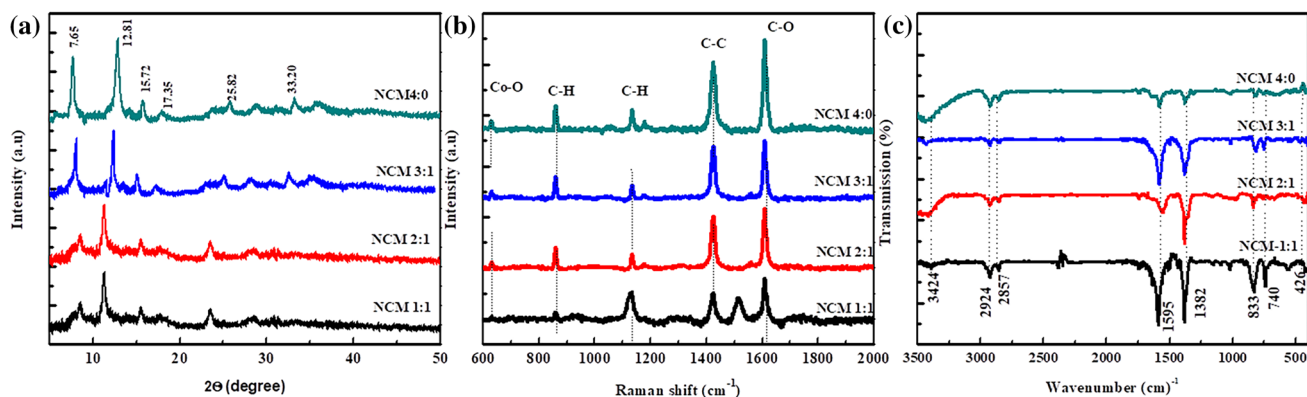


**Fig. 2** Structural characterization of Ni-Co MOF. (a) XRD patterns of prepared Ni-Co MOF materials. (b) Raman patterns of Ni-Co MOFs. (c) FTIR spectra of Ni-Co MOFs.

Since the Co atom has a higher atomic radius (2 Å) than the Ni atom (1.63 Å).<sup>42</sup> So the crystallinity of the samples is affected and the interplanar spacing increases with the addition of Ni atoms and the  $2\Theta$  values of diffraction peaks increase the interplanar spacing increases as shown in Table 1. Interplanar spacing is calculated by using Bragg's law for Eq. 5

$$d = \frac{n\lambda}{2\sin\Theta} \quad (5)$$

where  $d$  is the interplanar spacing,  $n$  is the order of diffraction,  $\lambda$  is the wavelength of incident x-ray,  $\Theta$  is the peak position.

The Raman spectrum of Ni-Co MOF has been studied. The nature of peaks is shown in Fig. 2b. The intense peaks observed at 1609  $\text{cm}^{-1}$ , 1514  $\text{cm}^{-1}$ , and 1428  $\text{cm}^{-1}$  are bounded by the C=C and C=O vibration of the benzene ring. Two modes are present in these carboxylate groups which are symmetric and asymmetric stretching modes. In addition intense bands at 1133  $\text{cm}^{-1}$ , 859  $\text{cm}^{-1}$  are associated with deformation modes in the C-H bonds, and less intense peaks observed at 628  $\text{cm}^{-1}$  approximate Co-O vibration which is specified by synthesized Ni-Co MOF material. These results are in excellent agreement with the demonstration reported in the literature, hence confirming the formation of Ni-Co MOF.<sup>43,44</sup> The intensity of Raman lines strongly depends upon the material concentration, since as the concentration of nickel ions increases, the intensity of peaks also gradually increases.

The formation of Ni-Co MOFs and their composites were further confirmed by FT-IR spectroscopy as an essential factor for obtaining a variety of information functional groups and chemical bonds present in the structure. Figure 2c shows the FT-IR spectra of NCM 1:1, NCM 2:1, NCM 3:1, and NCM 4:0. The peaks at 3423  $\text{cm}^{-1}$  and

2917  $\text{cm}^{-1}$ , 2856  $\text{cm}^{-1}$  describe the stretching vibration of OH<sup>-</sup> and CH groups. Asymmetric and symmetric (-COO-) stretching vibration of organic ligands of coordination of the metal center of Ni-Co MOF show peaks at 1554  $\text{cm}^{-1}$  and 1382  $\text{cm}^{-1}$ . Also, the difference between these two bands indicates that the -COO group of terephthalic acid is coordinated to Ni<sup>2+</sup> or Co<sup>2+</sup> or Ni<sup>2+</sup>/Co<sup>2+</sup> via a bidentate mode. The aspects of peaks Ni-O and Co-O at 422  $\text{cm}^{-1}$  are similar to the creation of a metal-oxo bond between the nickel and cobalt atoms and the carboxylic group of the organic ligand. Other peaks at 748  $\text{cm}^{-1}$  and 840  $\text{cm}^{-1}$  are peaks of the benzene ring pair.<sup>45,46</sup> All of these absorption bands are present even in the case of NCM 1:1, NCM 2:1, NCM 3:1 and NCM 4:0, and it can be seen from the figure that there is a slight change in the wavenumbers. Structural elucidation by FT-IR confirms the successful formation of Ni-Co MOFs. The peaks of the NCM 1:1 to NCM 4:0 samples show a slight shift relative to the NCM 1:1 sample possibly due to a coordination interaction between the nickel and cobalt bonds in the bimetallic sample.<sup>47</sup> Furthermore, the samples show peaks in a similar range confirming that similar chemical bonds are present in the samples. Overall FT-IR results confirm that nickel, cobalt, and water are present in the samples. The above results support XRD analysis and confirm the formation of Ni-Co MOF.

Here, SEM is used to observe the morphological evolution in the nickel-cobalt metal–organic framework with the change of nickel ratios during the synthesis. The expected morphological change is observed due to the change in the molar ratio of nickel as shown in Fig. 3. The nickel-cobalt material (NCM 1:1 sample) shows a flower-like structure composed of a large number of connected nanosheets. The image shows a compact connection between the nanosheets like microspheres (Fig. 3a and b).<sup>48,49</sup> In addition, the concentration of Ni ions increased, the flake-like

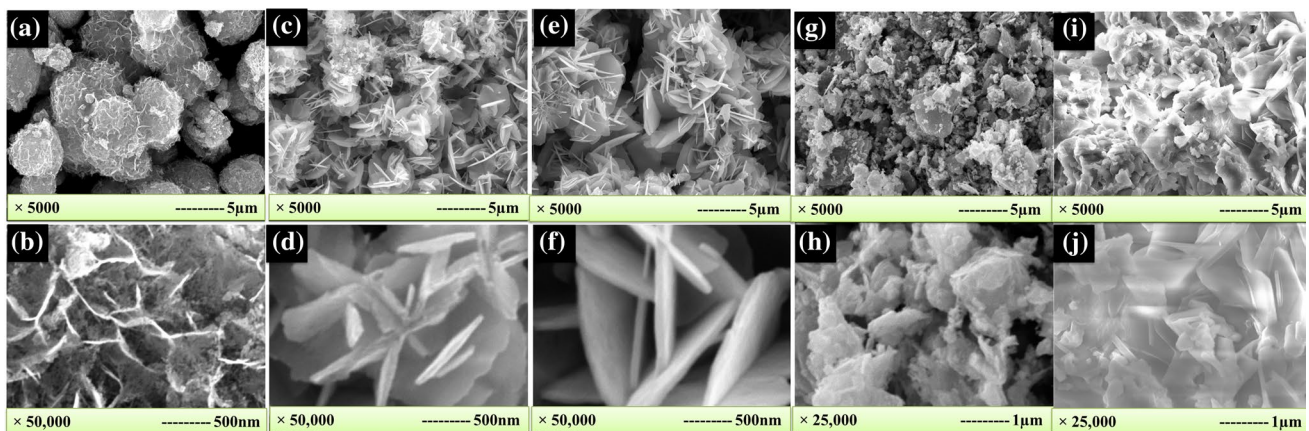


**Fig. 3** SEM images of Ni-Co MOFs prepared at different concentrations (a and b) NCM 1:1, (c and d) NCM 2:1, (e and f) NCM 3:1 and (g and h) NCM 4:0, (i and j) NCM 0:1.

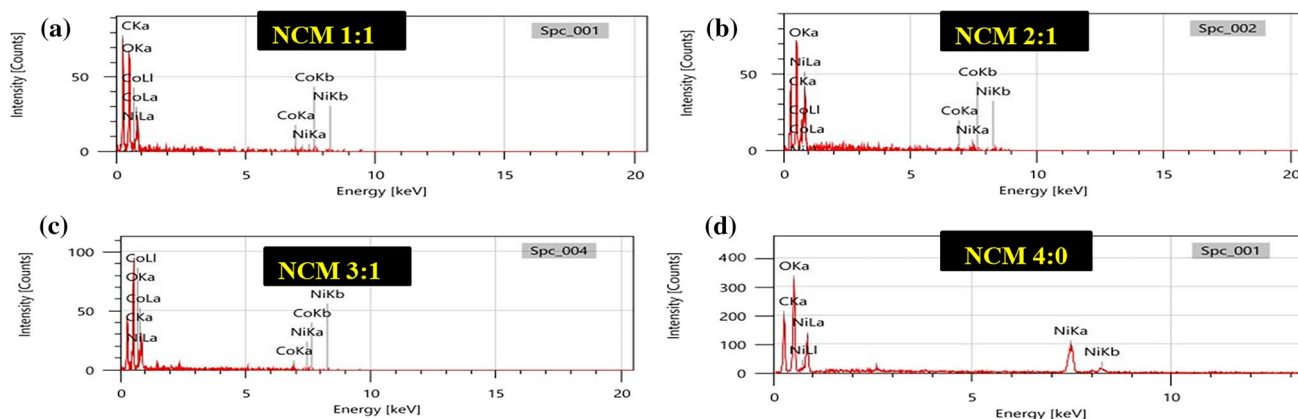


**Fig. 4** EDS spectra of the (a) NCM 1:1, (b) NCM 2:1, (c) NCM 3:1 and (d) NCM 4:0.

**Table II** EDS element content distribution chart

Element	C	O	Ni	Co	Total mass (%)
NCM 1:1	18.05	23.22	23.45	35.28	100
NCM 2:1	17.58	19.37	51.21	11.84	100
NCM 3:1	4.82	15.82	52.60	26.66	100
NCM 4:0	33.88	37.63	28.49	00	100

structure appeared more clearly, and the flakes became more homogeneous, as shown in Fig. 3c and d. SEM also revealed that NCM 2:1 exhibits good dispersion, uniform size, and thinner thickness so it can transport more electrically active sites, shorten the charge diffusion channel and increase the charge transfer rate.<sup>50</sup> After the Ni ion concentration increased, it could be observed that the flake-like structure of the Ni-Co MOF expanded and the arrangement was regular and porous, especially for the NCM 3:1 sample shown in Fig. 3e and f. The flake's width is larger than that of the NCM 2:1 sample. Hence, electrochemical performance gradually decreases as Ni content increases. It should be noted that the micro-flakes at the top of the NCM 4:0 sample agglomerate, destroying their structure, when the cobalt content is further removed, as shown in Fig. 3g and h. Figure 3i and j shows that the internal structure of nanoflakes is more equally distributed in a scattered way than the aggregated state of Ni-MOF. The controlled synthesis of Ni-Co MOFs using the solvothermal/hydrothermal method has been reported by several authors.<sup>43</sup> They clearly showed that the microstructure depends on the ion concentration, the reaction temperature, and the solvent or solvent mixture used to prepare the solution. Energy dispersive spectroscopy (EDS) mapping shows the presence of nickel, cobalt, carbon, and oxygen present in synthesized Ni-Co MOF. Figure 4 shows the weight percent of elements in the prepared sample. The morphology of MOF shows an arrangement of C and O using

**Table III** BET surface area, pore volume and mean pore diameter of NCM 1:1, NCM 2:1, NCM 3:1 and NCM 4:0, obtained using the  $N_2$  adsorption–desorption isotherms

Sample code	BET surface area ( $m^2/g$ )	Adsorption average pore radius (nm)
NCM 1:1	36.62	1.63
NCM 2:1	67.46	4.097
NCM 3:1	45.87	9.45
NCM 4:0	15.64	33.28

terephthalic acid as an organic linker. These results show the four elements compressed in the Ni-Co MOF structure. The percentage of elements is shown in Table II. The elemental data of the synthesized Ni-Co MOF is in agreement with the result given by Da et al.<sup>51</sup>

The surface manipulation and pore size of Ni-Co MOFs using four different samples were investigated by  $N_2$  adsorption–desorption measurements. At the same time, the morphology of the synthesized materials has a strong influence on the specific surface area, pore size, and pore volume. The BET-BJH data of the samples are presented in Table III and Fig. 5a–d. NCM 2:1 has the highest specific surface area of  $67.46 m^2/g$  and a total pore volume of  $0.2089 cm^3/g$ . The highest specific surface could be due to the more open porous structure formed by the flake-like structure of NCM 2:1, which is consistent with SEM images. Meanwhile, the synergistic effect of Ni and Co ions can effectively increase the specific surface area of NCM materials.<sup>7</sup> As with previous literature reviews, the high specific surface area and large pore volume are usually associated with better electrochemical behavior. On the one hand, it ensures a larger contact area between the electrodes and the electrolyte; on the other hand, it offers freer buffer voltage spaces during the charging and discharging cycles. However, as the amount of Ni increases, the structure of the material is destroyed,

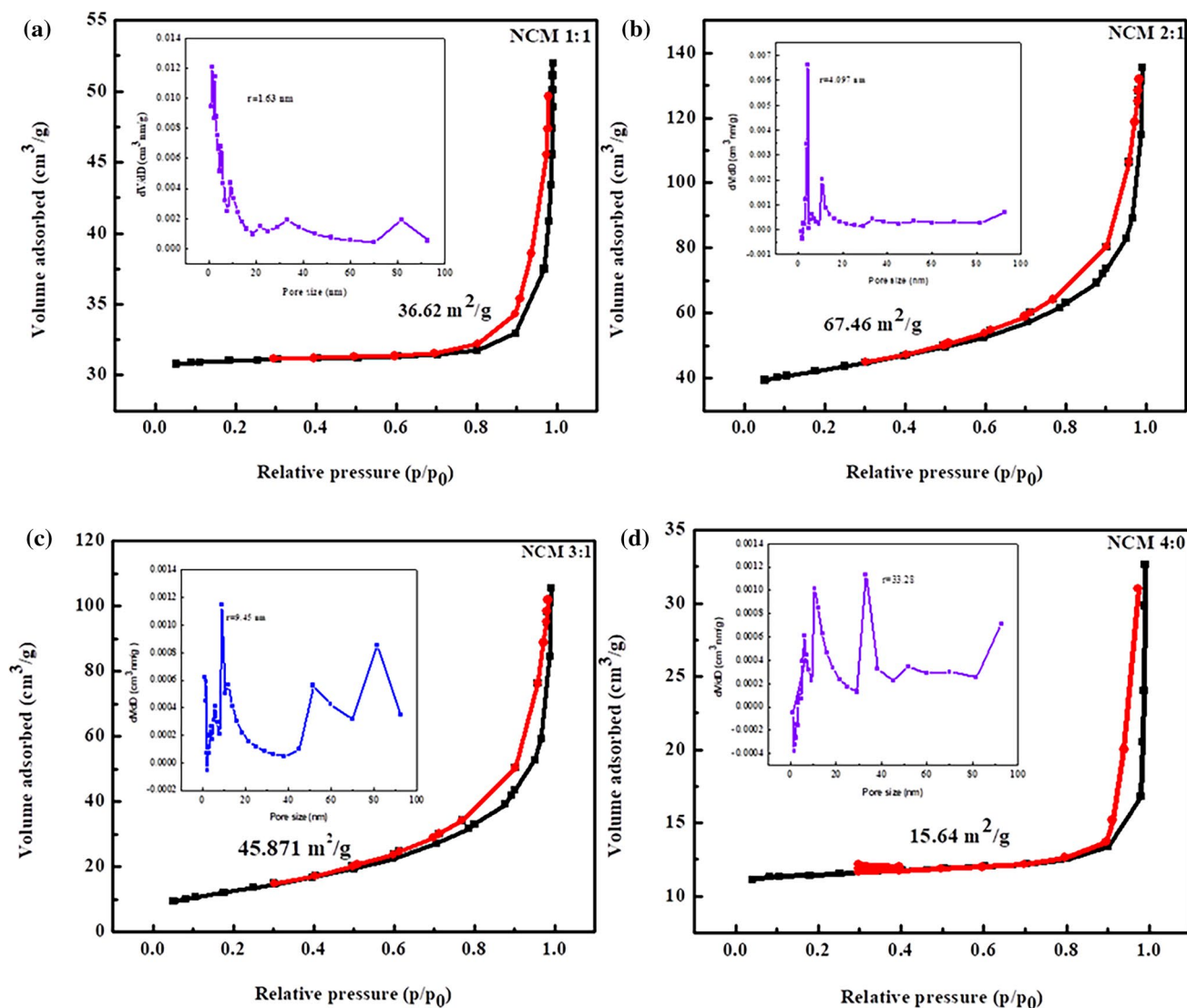


**Fig. 5** Nitrogen adsorption–desorption isotherms for (a) NCM 1:1, (b) NCM 2:1, (c) NCM 3:1 and (d) NCM 4:0. Inset shows the corresponding pore size distribution curves.

which in turn causes a decrease in specific surface areas, which corresponds to a decrease in electrochemical performance. When the Ni/Co molar ratio reaches a level where Ni and Co have an equivalent effect on the microstructure of Ni/Co MOFs, the MOFs exhibit distinct characteristics, and NCM 2:1 might belong in this case. However, the morphology of NCM 2:1 is completely different from other types. Its nanoflakes are considerably small and decorated with particle-like features (Fig. 3c and d). It is also revealed that NCM-2:1 has good dispersion, uniform size, and thinner thickness which can promote a large surface area. Different levels of stress and ability may play an important role in this morphological change. Surprisingly, NCM 3:1 recovered the nanoflake morphology,

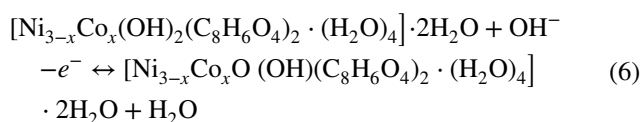
which can be explained by the fact that Ni is the dominant metallic element in NCM 3:1 and the effect of Co on the nanoflake size is relatively lower than NCM 2:1 so surface area decreases. Also, pore size distribution is another important factor affecting electrochemical performance.<sup>7</sup> However, if the pores are too large, the effectiveness of the active ingredient will be reduced. Therefore, a reasonable pore size distribution is very important to modify the electrochemical performance. Furthermore, it is reported that when MOFs have microparticles with a diameter of less than 2 nm, the transport of electrolyte ions is blocked. However, if the pores are too large, the effectiveness of the active ingredient is reduced. Therefore, a reasonable pore size distribution is very important to modify the electrochemical performance. The pore size of the synthesized



sample NCM 2:1 is concentrated at 2–5 nm, which is close to the ideal ion transport channel of supercapacitors.<sup>33</sup> Therefore, in terms of specific surface area and pore size distribution, NCM 2:1 is theoretically expected to exhibit better electrochemical performance as battery-like electrode materials.

### Effect of Different Concentrations on Electrochemical Performance of Ni-Co MOF

The effect of different concentrations on the electrochemical performance of Ni-Co MOF was studied with the help of a three-electrode system. For this study, silver chloride (Ag/AgCl) was used as the reference electrode and platinum wire as the counter electrode. For electrochemical measurements, a potential window range of 0–0.8 V and scan rate from 5 mV/s to 100 mV/s were used to test the performance in nickel cobalt metal–organic framework electrodes. Electrochemical testing of synthesized material was carried out using a 1.0 M KOH electrolyte system. The 1 cm<sup>2</sup> area of the working electrode is embedded in the electrolyte for precise electrochemical measurements. Electrochemical studies were performed using a Nova 2.1.5 workstation. Five-electrode CV curves of NCM 1:1, NCM 2:1, NCM 1:1, NCM 4:0 and NCM 0:1 at the same scan rate of 5 mV/s are shown in Fig. 6a. All CV curves clearly show the shape of the battery-like activity, which is attributed to a faradaic redox reaction in the raw phase of the electrode material. In the CV curves of all Ni-Co-based MOF electrodes, a pair of well-separated faradaic redox peaks was observed with sharp peaks and a relatively large potential gap. This is a characteristic of battery-like behavior. The intercalation of OH<sup>-</sup> ions from the electrolyte to the surface of nickel cobalt MOF material takes place at the time of charging and deintercalates during discharging. This can be explained by the following reaction mechanism.<sup>20,38</sup>



The improved performance may be due to the strong synergies of Co<sup>2+</sup> and Ni<sup>2+</sup>. In particular, the NCM 2:1 electrode showed the maximum CV curve area even when the sampling rate was increased to 100 mV/s.<sup>46,52</sup> Figure 6c shows the CV response of NCM 2:1 at different scan rates ranging from 5 to 100 mV/s. The high capacity of NCM 2:1 is attributed to the redox reactions participated by both nickel ions and cobalt ions in the charge/discharge process.

Figure 6b shows the GCD curves of the four electrode samples at a current density of 4 mA/cm<sup>2</sup>. The GCD curves at different current densities are depicted in Fig. 6d. In

particular, the nonlinear GCD curves exhibit some symmetric background, which proves that these electrodes have good electrochemical performance. The interpretation of the discharge curve can be divided into two views: a very small voltage drop and a charge transfer response of the working electrode. When the voltage reaches the highest point, the current drops sharply representing the beginning of discharge curves, indicating that the voltage drop of the electrode is due to its internal resistance.<sup>53</sup> It is also well proven that the 2:1 NCM has the longest discharge time and the best electrochemical behavior. The larger interface area of the 2:1 NCM effectively promotes charge transfer, thereby reducing the internal resistance of the working electrode. A longer charge–discharge time exhibits a more noticeable specific capacitance, as determined by Eq. 1. In Fig. 6c, the maximum specific capacitance of 1385 F/g belongs to NCM 2:1 in 4 mA/cm<sup>2</sup>. At the same current density, NCM 1:1, NCM 3:1, NCM 4:0 and NCM 0:1 revealed specific capacitance of 967 F/g, 1192 F/g, 677 F/g, 453 F/g. Furthermore, the specific capacitance decreases with increasing current density, which might be related to ion migration limitations in active materials is shown in Table IV. Significant OH<sup>-</sup> ions must intercalate quickly at the electrode/electrolyte interface at high current densities, but the short charging time, low concentration, and poor accessibility of OH<sup>-</sup> ions cannot match this demand. The specific capacitance of the Ni-Co MOF electrode was calculated from charge–discharge curves by using Eq. 7:

$$C_p = \frac{I\Delta t}{m\Delta v} \quad (7)$$

where  $I$  is current density (mA),  $m$  is active mass (g),  $\Delta t$  is discharge time (s), and  $\Delta v$  is the potential window (V).<sup>54</sup>

The EIS results shown in Fig. 6e also confirmed this. In particular, the radius of the semicircle indicates the charge transfer resistance (Rct) used to calculate the charge transfer capacity between the electrode and the electrolyte. The smaller radius of the semicircle reflects faster charge transfer at the electrode/electrolyte interface. Compared with NCM 2:1, the other electrode materials, namely NCM 1:1 NCM 3:1, NCM 4:0, and NCM 0:1, have larger Rct, resulting in low electrochemical activity as shown in Table V. However, with increasing Ni content in MOF, the Rct value of Ni-Co MOF excluding NCM 2:1 gradually decreased, observing improved electrochemical behavior due to efficient electronic tuning. Furthermore, the straight line can also be used to evaluate the capacitance performance. The more vertical line of NCM 2:1 indicates better capacitive behavior associated with faster ion diffusion, suggesting that the addition of Ni also affects the pore structure of the Ni-Co MOF. Finally, as the amount of Ni decreases, the crystalline grains of the Ni-Co MOF become smaller, thereby increasing the surface area and thus improving the capacitance efficiency.<sup>55</sup>

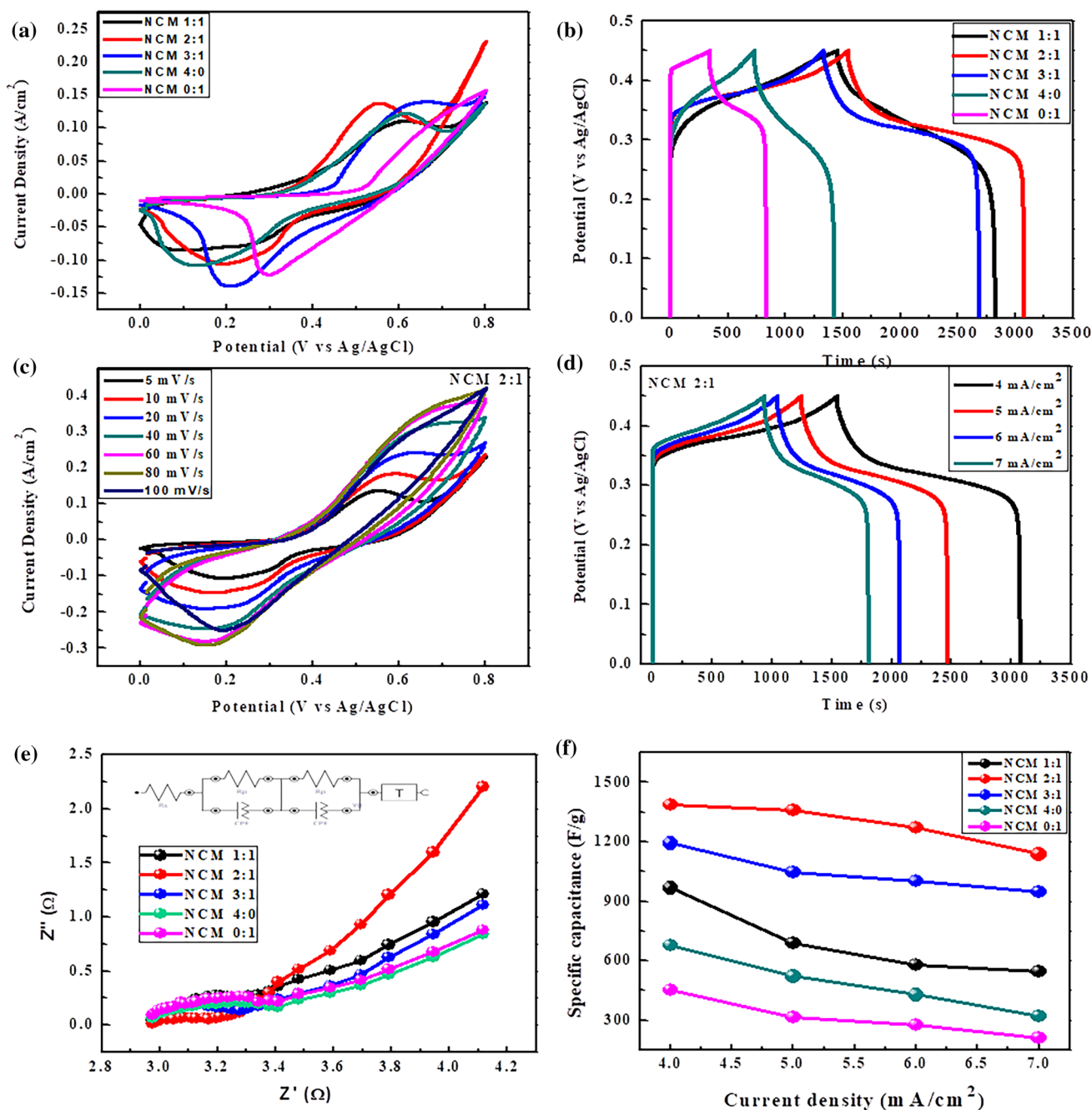


**Fig. 6** Electrochemical performance of Ni-Co MOF electrodes: (a) CV curves of NCM electrodes scanned at 5 mV/s, (b) GCD curves of NCM electrodes at 4A/g, (c) CV plots of NCM 2:1 electrode, (d)

GCD graphs of NCM 2:1 electrode, (e) EIS plot of NCM electrodes, (f) calculated specific capacitances versus current densities of NCM electrodes.

Figure 6f presents a comparison of the electrochemical behaviors between different Ni-Co MOF electrodes. Apparently, the NCM 2:1 electrode (2:1 Ni-Co MOF ratio) exhibits higher capacitance than other NCM electrodes. Furthermore, NCM 2:1 exhibited the highest specific capacitance of 1385 F/g at 4 mA/cm<sup>2</sup> while maintaining 1137 F/g at 7 mA/cm<sup>2</sup>, demonstrating its good throughput performance. The excellent electrochemical properties of NCM 2:1 may be the

result of flake morphology with a more open hierarchy and the highest specific area, which facilitates electron transport and ion diffusion of electrolytes during redox reactions. The cyclic stability is also an important parameter to study the lifetime of the supercapacitor electrode. The analysis of the NCM 2:1 electrode was carried out across 3000 CV cycles at the scan rate of 100 mV/s in 1 M KOH electrolyte. Figure 6g shows the graph of capacitance retention versus the number

**Table IV** Values of specific capacitance, energy density and power density calculated from charge discharge curves at different current densities

Sr. no.	Sample code	Current density (mA/cm <sup>2</sup> )	Specific capacitance (F/g)	Energy density (Wh/kg)	Power density (W/kg)
1	NCM 1:1	4	967	27.19	53.53
2		5	689	121.37	75.52
3		6	681	19.15	97.93
4		7	685	16.26	131
1	NCM 2:1	4	1385	38.95	141
2		5	1358	38.19	165.05
3		6	1270	35.71	182.4
4		7	1137	31.97	197.9
1	NCM 3:1	4	1192	33.52	88.46
2		5	1253	31.24	111.18
3		6	1185	29.65	134.62
4		7	1148	25.76	156.61
1	NCM 4:0	4	677	19.04	67
2		5	521	14.65	124.97
3		6	428	12.03	12.03
4		7	320	9	161.87
1	NCM 0:1	4	453	12.74	89.93
2		5	314	9.7	81.58
3		6	275	7.5	75.31
4		7	212	6.9	83.63

**Table V** Comparison of charge transfer resistance of different material

Sample (Rs)	Charge transfer resistance (Rct)	Series equivalent resistance
NCM 1:1	0.3042 $\Omega$	2.9751 $\Omega$
NCM 2:1	0.1865 $\Omega$	2.9731 $\Omega$
NCM 3:1	0.2737 $\Omega$	2.9771 $\Omega$
NCM 4:0	0.4266 $\Omega$	2.9787 $\Omega$
NCM 0:1	0.5685 $\Omega$	2.9811 $\Omega$

of cycles for the Ni-Co MOF electrode. As shown in Fig. 7a, the stability plot for Ni-Co MOF demonstrates 88.4% capacitance retention after 3000 CV cycles. The inset figure shows the cyclic voltammetry curves of the first and 3000th cycles. After 3000 CV cycles, only an 11.6% decrease in the initial value of capacitance occurred which is due to the dissolution of ions in an aqueous electrolyte. The Ni-Co MOF electrode showed 88.4% capacitance retention, respectively. To evaluate the performance of supercapacitors, energy density and power density are two key factors determined using the Ragone plot. This graph shows the correlation between three electrode system energy density and power density for Ni-Co MOF (NCM 1:1, NCM 2:1, NCM 3:1, NCM 4:0, and NCM 0:1) as shown in Fig. 7b, which is calculated from

Eqs. 2 and 3. A higher energy density of 38.95 Wh/kg at the power density of 141 W/kg was observed for the NCM 2:1 electrode as compared to NCM 1:1, NCM 3:1, NCM 4:0, and NCM 0:1 electrodes. The energy densities of 27 W/kg, 33 W/kg, and 19 Wh/kg at the power densities of 53 W/kg, 88 W/kg, and 67 W/kg were observed for NCM 1:1, NCM 3:1, and NCM 4:0 electrodes at the current density of 4 mA/cm<sup>2</sup>, respectively. These results showed that NCM 2:1 has much better electrochemical performance than NCM 1:1, NCM 3:1, NCM 4:0 and NCM 0:1 power density due to its high specific capacity (1385 F/g) and energy density of 38.95 Wh/kg 141 W/kg. The good cycling stability of the NCM 2:1 electrode was reflected in its high structural stability, which could help provide more channels for electron transport and make the more electroactive surface area accessible to the electrolyte.

To better understand the charge transfer rate of the NCM 2:1 electrode, we applied the power law to determine the contribution of charge accumulation in the capacitive and diffusion-controlled response based on the CV curve. The peak current ( $i_p$ ) can be associated with the sampling rate ( $v$ ) using the Eq. 8:

$$i_p = av^b \quad (8)$$

where  $a$  and  $b$  are the tuning parameters. The value of  $b$  is particularly 0.5 or 1; when  $b = 0.5$ , charge storage is mainly

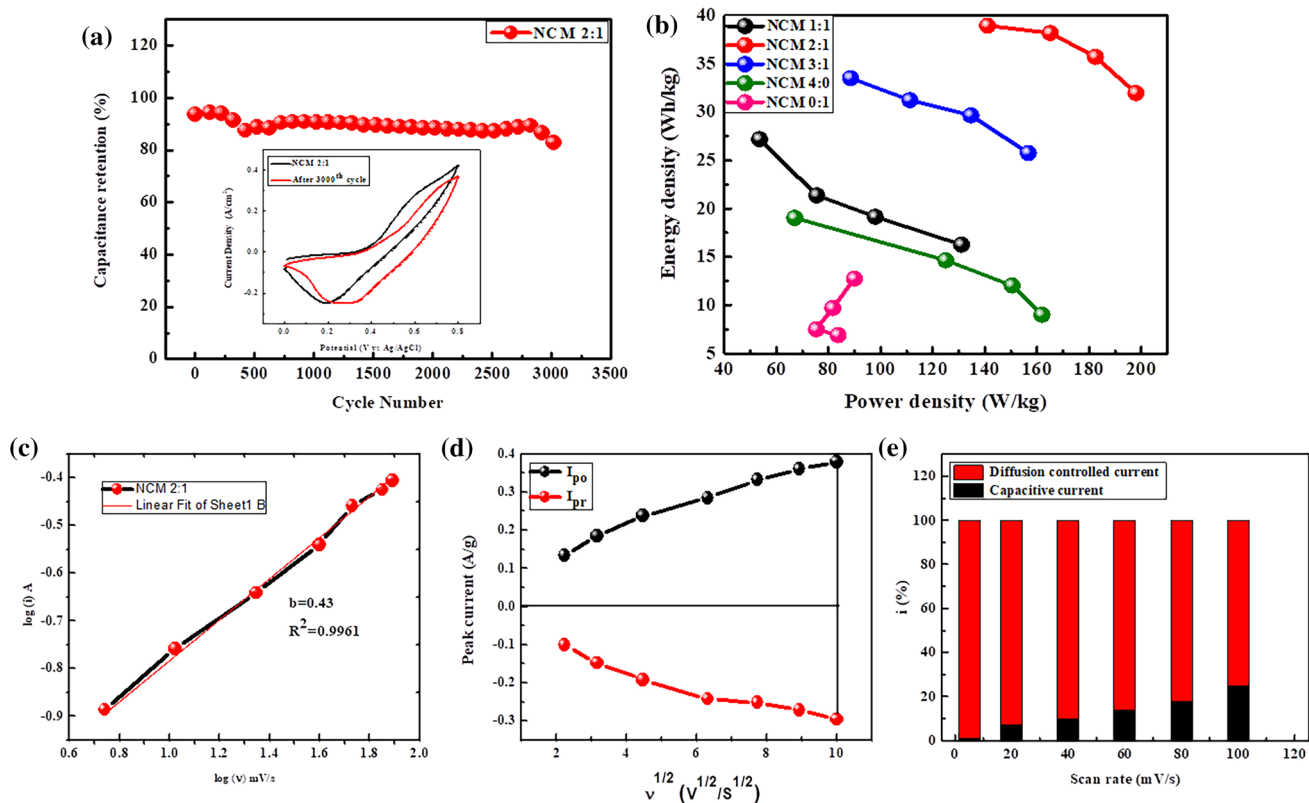


**Fig. 7** (a) Cyclic performances of NCM 2:1 electrode at 100 mV/s, (b) Ragone plot of NCM samples, (c)  $b$  value from the fitted lines (logarithm peak current against logarithm of scan rate), (d) plot of

peak current versus square root of scan rate, (e) diffusion contribution and capacitive contribution as a function of different scan rates.

a result of diffusion control, and when  $b = 1$ , charge storage is the result of the capacitive process. The  $b$ -value can be evaluated from the slope of the  $\log(i)$  versus  $\log(v)$  curve, as shown in Fig. 7c. The  $b$  value obtained with the NCM 2:1 electrode is 0.43, indicating the superiority of the diffusion rate-determining charge storage process over the capacitive process. As shown in Fig. 7d, the mechanism of electrolyte diffusion during the charge storage process was studied based on the relationship between peak oxidation and reduction currents and the square root of the sampling rate. The peak current increases in proportion to the square root of the sample rate, and further shows the diffusion of electrolyte ions during the electrochemical process of the NCM 2:1 electrode.<sup>56</sup> To further evaluate the contribution of the capacitive and diffusion rate-determining process to charge storage, the total charge stored at a given potential is a combination of currents from a capacitive ( $k_1 v$ ) process and a diffusion rate-determining ( $k_2 v^{1/2}$ ) process.

Therefore, the power law is determined by Eq. 9.

$$i_p = k_1 v + k_2 v^{1/2} \quad (9)$$

where  $i_p$  is the peak current, and  $k_1$  and  $k_2$  are coefficients for capacitance current and diffusion-controlled current, respectively. Figure 7e shows the contribution of the capacitive and diffusion-controlled charge storage of the NCM 2:1 electrode at different scan rates. Results confirm that the dominant charge storage mechanism of the NCM 2:1 electrode is based on the diffusion-controlled process, not the capacitive process.<sup>57,58</sup>

To further evaluate the practical applicability of the NCM 2:1 material, we measured energy density and power density using two-electrode systems. The cyclic voltammogram is carried out at a cell voltage of 0–0.6 V and various sweep rates of 10–100 mV/s as shown in Fig. 8a. Galvanostatic charge–discharge tests at various current densities of 1–4 mA/cm<sup>2</sup> with cell voltages ranging from 0.0 V to 0.45 V were carried out to verify the energy storage behavior, as shown in Fig. 8b. At higher current densities (4 mA/cm<sup>2</sup>) the SSC device's GCD plots demonstrate nonlinear charge–discharge curves, which point to the power device's excellent capacitive characteristics and desired rapid charge–discharge qualities. At a current density of 1 mA/cm<sup>2</sup>, the device has a maximum specific capacitance 280 F/g. The cycling stability of the symmetric device is recorded over 10,000 cycles

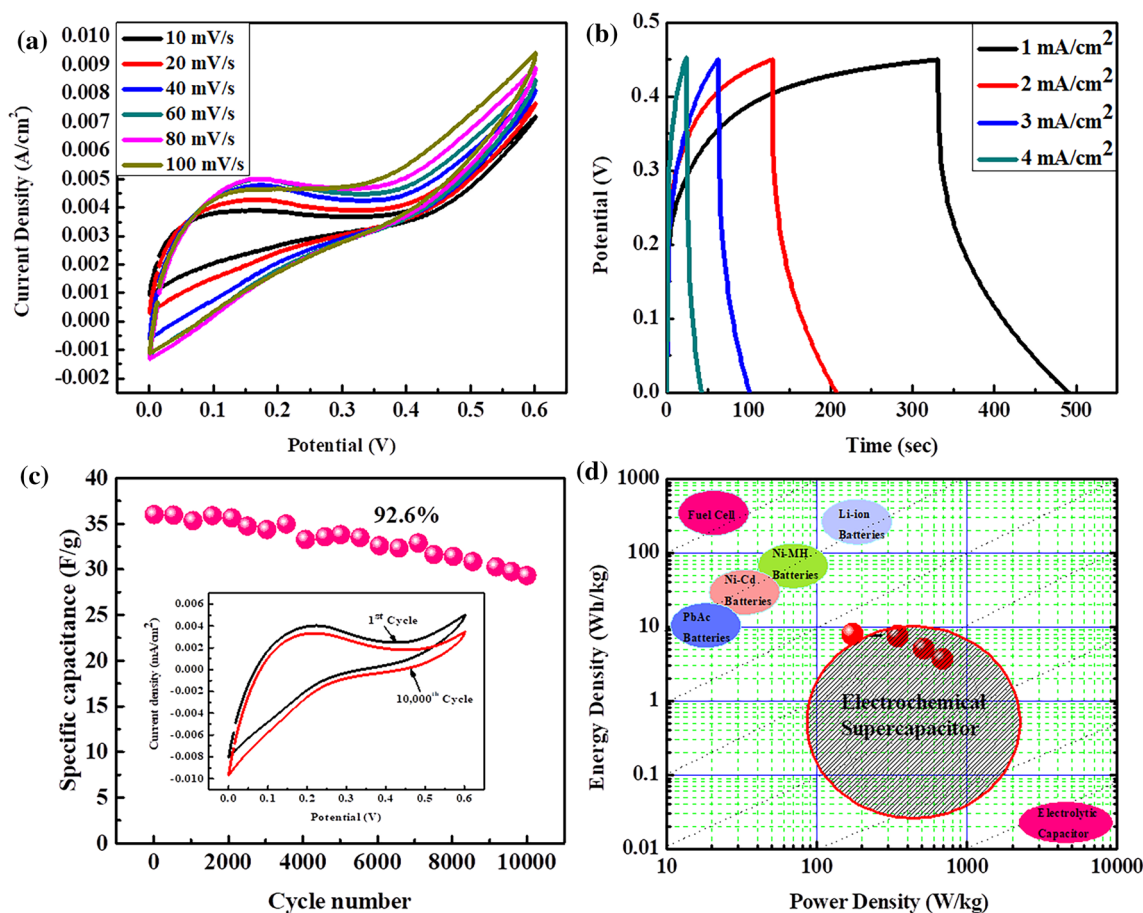


**Fig. 8** Symmetric device performance. (a) CV curves at different scan rates, (b) GCD curves at different current densities, (c) plot of specific capacitance versus cycle number, with inset showing stability difference between the first cycle and 10,000th cycle, (d) Ragone plot of device.

as presented in Fig. 8c. The symmetric device shows 92.6% capacitance retention over 10,000 cycles indicating excellent cycle stability. The energy and power densities are also evaluated for NCM 2:1//NCM 2:1 symmetric device using Eqs. 3 and 4 and are presented in Fig. 8d. The energy density of 7.8 Wh/kg can be achieved at a power density of 173.07 W/kg and 3.65 Wh/kg is maintained even at a high power density of 692.30 W/kg.

A comparative study of the electrochemical properties of hydrothermally cultured Ni-Co MOF electrodes (NCM 1:1, NCM 2:1 and NCM 3:1, and NCM 4:0) was performed using radar display, as shown in Fig. 9. Each peak displays parameters such as crystal size, and SSA of the Ni-Co MOF samples and obtained supercapacitive parameters such as specific surface area, pore radius, energy density, power density, series resistance, and charge transfer resistance of the respective materials. The integral area under the curve displays the electrochemical performance of the NCM samples. From Fig. 9, it can be observed that the integral area of NCM 2:1 is remarkable compared with NCM 1:1, NCM 3:1, and NCM 4:0. It is confirmed that the small crystal

size, large SSA, and minimum series resistance of the NCM 2:1 contribute to the increased specific capacitance, power density, power density, and cyclic stability. These results show that NCM 2:1 has a higher specific capacitance (1385 F/g), an energy density of 38.95 Wh/kg, and a power density of 141 W/kg, so it is better than NCM 1:1, NCM 3:1, and NCM 4:0. It shows that it has much better electrochemical performance. The excellent cycling stability of the NCM 2:1 electrode is reflected in its high structural stability, providing more channels for electron transport and creating more electroactive surface area accessible to the electrolyte.

## Conclusion

In summary, nickel-cobalt metal–organic framework flakes with similar structures have been successfully synthesized by a hydrothermal method. NCM 2:1 has the highest specific capacitance of 1385 F/g at 4 mA/cm<sup>2</sup> and holds 1137 F/g even at 7 mA/cm<sup>2</sup>. The improved electrochemical performance can be attributed to a flake-like structure with a more

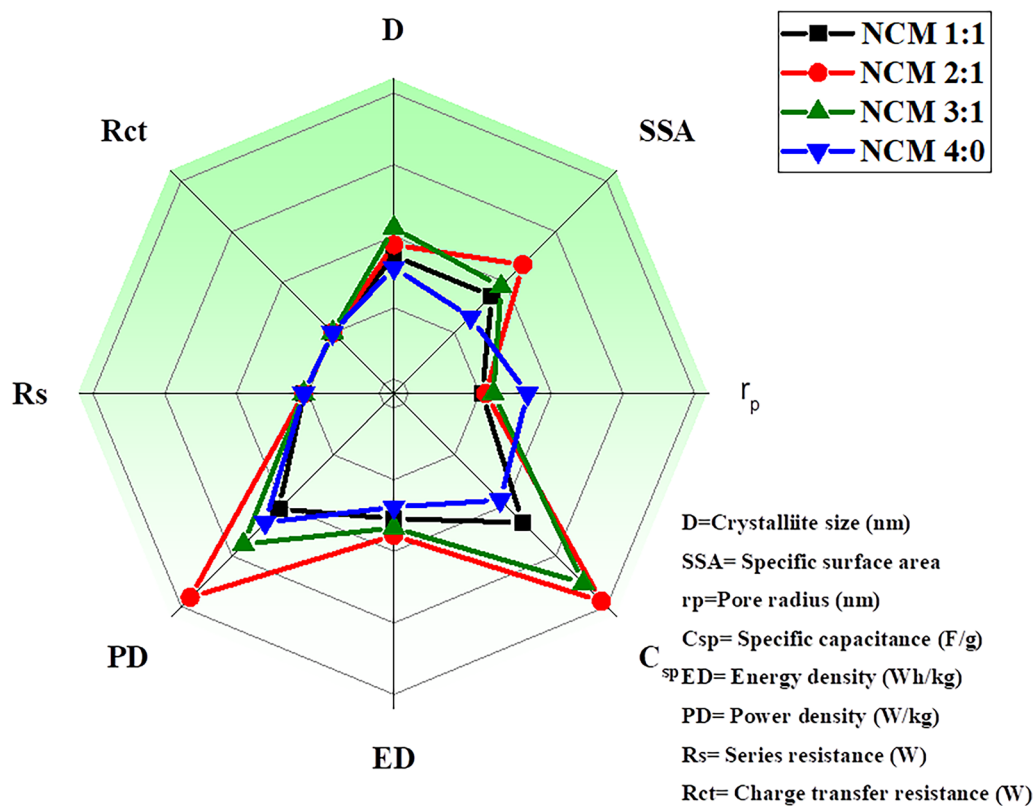


**Fig. 9** Radar plot for comparative study of Ni-Co MOF electrodes based on supercapacitive properties.

open structure and larger surface area, increasing the contact area between the electrode and the electrolyte while shortening the path length for ion transport. The synergistic effect of the Ni-Co MOF electrode between  $Ni^{2+}$  and  $Co^{2+}$  also contributes to the improvement of conductivity. The concentration of empty holes has been reported to play an important role in the conductivity of nickel-based materials. Because of the similar size of  $Co^{2+}$  radius (0.065 nm) and  $Ni^{2+}$  radius (0.069 nm), relatively small  $Ni^{2+}$  ions diffuse into Co-MOF, partially substituting  $Co^{2+}$  ions for more. It can form many  $Co^{2+}$  vacancies. This action may increase the empty holes in the Ni concentration, increase the MOF, and improve the conductivity of the MOF. The energy density of 7.8 Wh/kg can be achieved at a power density of 173.07 W/kg and 3.65 Wh/kg is maintained even at a high power density of 692.30 W/kg. All these results show that Ni-Co MOFs of this type have promise as electrodes in supercapacitors.

**Acknowledgments** Author Amruta D. Salunkhe would like thank the Chhatrapati Shahu Maharaj Research Training and Human Development Institute (SARTHI), Pune (Government of Maharashtra), for the financial support under the Chhatrapati Shahu Maharaj National Research Fellowship 2021. The authors are thankful to the Department of Physics at the Yashwantrao Chavan Institute of Science, Satara (Autonomous), and the Rayat Institute of Research Development (RIRD), Satara, for the laboratory facility.

**Author Contributions** ADS: Conceptualization, Methodology, and Writing—original draft, PKP: Data curation, Methodology APT: Supervision.

**Data Availability** All data generated or analysed during this study are included in this manuscript will be freely available to any researcher wishing to use them for non-commercial purpose.

**Conflict of interest** The authors declare that they have no known competing financial interests or personal relationships that could have appeared to influence the work reported in this paper.

## References

1. K. Sharma, A. Arora, and S.K. Tripathi, Review of supercapacitors: materials and devices. *J. Energy Stor.* 21, 801–825 (2019).
2. C.V.V. Muralee Gopi, R. Vinodh, S. Sambasivam, I.M. Obaidat, and H.J. Kim, Recent progress of advanced energy storage materials for flexible and wearable supercapacitor: from design and development to applications. *J. Energy Stor.* 27, 101035 (2020).
3. D. Zheng, W. Hao, S. Xun, G. Xin, Z. Jie, T. Wenli, F. Hao, W. Hongjing, and Y. Yadong, Ultrathin Mn Doped Ni-MOF nanosheet array for highly capacitive and stable asymmetric supercapacitor. *Chem. A Eur. J.* 71, 17149–17155 (2020).
4. Z.S. Iro, C. Subramani, and S.S. Dash, A brief review on electrode materials for supercapacitor. *Int. J. Electrochem. Sci.* 11(12), 10628–10643 (2016).

5. X.W. Liu, T.J. Sun, J.L. Hu, and S.D. Wang, Composites of metal–organic frameworks and carbon-based materials: preparations, functionalities and applications. *J. Mater. Chem. A* 4(10), 3584–3616 (2016).
6. V. Augustyn, P. Simon, and B. Dunn, Pseudocapacitive oxide materials for high-rate electrochemical energy storage. *Energy Environ. Sci.* 7(5), 1597–1614 (2014).
7. Y. Chen, D. Ni, X. Yang, C. Liu, J. Yin, and K. Cai, Microwave-assisted synthesis of honeycomblike hierarchical spherical Zn-doped Ni-MOF as a high-performance battery-type supercapacitor electrode material. *Electrochim. Acta* 278, 114–123 (2018).
8. Y. Zhao, J. Liu, M. Horn, N. Motta, M. Hu, and Y. Li, Recent advancements in metal organic framework based electrodes for supercapacitors. *Sci. China Mater.* 61(2), 159–184 (2018).
9. R.R. Salunkhe, K. Yuichiro, L.T. Nagy, H.S. Min, S. Ziqi, S.X. Dou, J.H. Kim, and Y. Yusuke, Fabrication of symmetric supercapacitors based on MOF-derived nanoporous carbons. *J. Mater. Chem. A* 2(46), 19848–19854 (2014).
10. B. Li, H.-M. Wen, Y. Yu, Y. Cui, W. Zhou, B. Chen, and G. Qian, Nanospace within metal–organic frameworks for gas storage and separation. *Mater. Today Nano* 2, 21–49 (2018).
11. D.G. Wang, Z. Liang, S. Gao, C. Qu, and R. Zou, Metal–organic framework-based materials for hybrid supercapacitor application. *Coord. Chem. Rev.* 404, 213093 (2020).
12. Q. Deng and R. Wang, Heterogeneous MOF catalysts for the synthesis of trans-4,5-diaminocyclopent-2-enones from furfural and secondary amines. *Catal. Commun.* 120, 11–16 (2019).
13. H.S. Wang, Y.H. Wang, and Y. Ding, Development of biological metal–organic frameworks designed for biomedical applications: from bio-sensing/bio-imaging to disease treatment. *Nanoscale Adv.* 2(9), 3788–3797 (2020).
14. M.L. Hu, S.A.A. Razavi, M. Piroozzadeh, and A. Morsali, Sensing organic analytes by metal–organic frameworks: a new way of considering the topic. *Chem. Front.* 7(7), 1598–1632 (2020).
15. Y.Y. Cai, Q. Yang, Z.Y. Zhu, Q.H. Sun, A.M. Zhu, Q.G. Zhang, and Q.L. Liu, Achieving efficient proton conduction in a MOF-based proton exchange membrane through an encapsulation strategy. *J. Membr. Sci.* 590, 117277 (2019).
16. Y. Xue, S. Zheng, H. Xue, and H. Pang, Metal–organic framework composites and their electrochemical applications. *J. Mater. Chem. A* 7(13), 7301–7327 (2019).
17. J.H. Dou, M.Q. Arguilla, Y. Luo, J. Li, W. Zhang, L. Sun, J.L. Mancuso, L. Yang, T. Chen, L.R. Parent, and G. Skorupskii, Atomically precise single-crystal structures of electrically conducting 2D metal–organic frameworks. *Nat. Mater.* 20(2), 222–228 (2021).
18. R.R. Salunkhe, J. Tang, N. Kobayashi, J. Kim, Y. Ide, S. Tomimaka, J.H. Kim, and Y. Yamauchi, Ultrahigh performance supercapacitors utilizing core-shell nanoarchitectures from a metal–organic framework-derived nanoporous carbon and a conducting polymer. *Chem. Sci.* 7(9), 5704–5713 (2016).
19. T. Wei, M. Zhang, P. Wu, Y.J. Tang, S.L. Li, F.C. Shen, X.L. Wang, X.P. Zhou, and Y.Q. Lan, POM-based metal–organic framework/reduced graphene oxide nanocomposites with hybrid behavior of battery-supercapacitor for superior lithium storage. *Nano Energy* 34, 205–214 (2017).
20. Y. Jiao, J. Pei, D. Chen, C. Yan, Y. Hu, Q. Zhang, and G. Chen, Mixed-metallic MOF based electrode materials for high performance hybrid supercapacitors. *J. Mater. Chem. A* 5(3), 1094–1102 (2017).
21. L. Zhang, X. Wang, R. Wang, and M. Hong, Structural evolution from metal–organic framework to hybrids of nitrogen-doped porous carbon and carbon nanotubes for enhanced oxygen reduction activity. *Chem. Mater.* 27(22), 7610–7618 (2015).
22. D.H. Yang, H.Y. Zhou, H. Liu, and B.H. Han, Hollow N-doped carbon polyhedrons with hierarchically porous shell for confinement of polysulfides in Lithium–Sulfur batteries. *iScience* 13, 243–253 (2019).
23. C. Wang et al., Electrospun metal–organic framework derived hierarchical carbon nanofibers with high performance for supercapacitors. *Chem. Commun.* 53(10), 1751–1754 (2017).
24. S. Sundriyal, H. Kaur, S.K. Bhardwaj, S. Mishra, K.H. Kim, and A. Deep, Metal–organic frameworks and their composites as efficient electrodes for supercapacitor applications. *Coord. Chem. Rev.* 369, 15–38 (2018).
25. Z. Li, Z. Xiao, S. Wang, Z. Cheng, P. Li, and R. Wang, Engineered interfusion of hollow nitrogen-doped carbon nanospheres for improving electrochemical behavior and energy density of Lithium–Sulfur batteries. *Adv. Funct. Mater.* 29(31), 1–12 (2019).
26. Y. Yan, P. Gu, S. Zheng, M. Zheng, H. Pang, and H. Xue, Facile synthesis of an accordion-like Ni-MOF superstructure for high-performance flexible supercapacitors. *J. Mater. Chem. A* 4(48), 19078–19085 (2016).
27. Y. Han, S. Zhang, N. Shen, D. Li, and X. Li, MOF-derived porous NiO nanoparticle architecture for high performance supercapacitors. *Mater. Lett.* 188, 1–4 (2017).
28. P. Du, Y. Dong, C. Liu, W. Wei, D. Liu, and P. Liu, Fabrication of hierarchical porous nickel based metal–organic framework (Ni-MOF) constructed with nanosheets as novel pseudo-capacitive material for asymmetric supercapacitor. *J. Colloid Interface Sci.* 518, 57–68 (2018).
29. S. Gao, Y. Sui, F. Wei, J. Qi, Q. Meng, and Y. He, Facile synthesis of cuboid Ni-MOF for high-performance supercapacitors. *J. Mater. Sci.* 53(9), 6807–6818 (2018).
30. W. Xuan, R. Ramachandran, C. Zhao, and F. Wang, Influence of synthesis temperature on cobalt metal–organic framework (Co-MOF) formation and its electrochemical performance towards supercapacitor electrodes. *J. Solid State Electrochem.* 22(12), 3873–3881 (2018).
31. D.Y. Lee, S.J. Yoon, N.K. Shrestha, S.H. Lee, H. Ahn, and S.H. Han, Unusual energy storage and charge retention in Co-based metal–organic-frameworks. *Microporous Mesoporous Mater.* 153, 163–165 (2012).
32. J. Yang, Z. Ma, W. Gao, and M. Wei, Layered structural Co-based MOF with conductive network frames as a new supercapacitor electrode. *Chem. A Eur. J.* 23(3), 631–636 (2017).
33. J. Wang, Q. Zhong, Y. Xiong, D. Cheng, Y. Zeng, and Y. Bu, Fabrication of 3D Co-doped Ni-based MOF hierarchical microflowers as a high-performance electrode material for supercapacitors. *Appl. Surf. Sci.* 483(March), 1158–1165 (2019).
34. G. Sriresh and A.S. Nesaraj, Chemical synthesis of Co and Mn co-doped NiO nanocrystalline materials as high-performance electrode materials for potential application in supercapacitors. *Ceram. Int.* 42(4), 5001–5010 (2016).
35. H. Gholipour-Ranjbar, M. Soleimani, and H.R. Naderi, Application of Ni/Co-based metal–organic frameworks (MOFs) as an advanced electrode material for supercapacitors. *New J. Chem.* 40(11), 9187–9193 (2016).
36. S. Maity, P.P. Das, and S.S. Mal, Decavanadate-graphene oxide nanocomposite as an electrode material for electrochemical capacitor. *Mater. Technol.* 00(00), 1–11 (2021).
37. K.B. Pisal, B.M. Babar, S.H. Mujawar, S.S. Mali, C.K. Hong, S.D. Sartale, and L.D. Kadam, MoS<sub>2</sub> nanosheets as bifunctional electrode for oxygen evolution reaction and electrochemical supercapacitor, (2022) pp. 1–16
38. F. Xu, N. Chen, Z. Fan, and G. Du, Ni/Co-based metal organic frameworks rapidly synthesized in ambient environment for high energy and power hybrid supercapacitors. *Appl. Surf. Sci.* 528, 146920 (2020).

39. C.R. Rawool, S.P. Karna, and A.K. Srivastava, Enhancing the supercapacitive performance of Nickel based metal organic framework-carbon nanofibers composite by changing the ligands. *Electrochim. Acta* 294, 345–356 (2019).
40. S.B. Dhavale, V.L. Patil, S.A. Beknalkar, A.M. Teli, A.H. Patil, A.P. Patil, J.C. Shin, and P.S. Patil, Study of solvent variation on controlled synthesis of different nanostructured NiCo<sub>2</sub>O<sub>4</sub> thin films for supercapacitive application. *J. Colloid Interface Sci.* 588, 589–601 (2021).
41. Q. Li, Y. Li, H. Peng, X. Cui, M. Zhou, K. Feng, and P. Xiao, Layered NH<sub>4</sub>Co<sub>x</sub>Ni<sub>1-x</sub>PO<sub>4</sub>·H<sub>2</sub>O (0 ≤ x ≤ 1) nanostructures finely tuned by Co/Ni molar ratios for asymmetric supercapacitor electrodes. *J. Mater. Sci.* 51(22), 9946–9957 (2016).
42. H. Gao, G. Wang, M. Yang, L. Tan, and J. Yu, Novel tunable hierarchical Ni-Co hydroxide and oxide assembled from two-wheeled units. *Nanotechnology* 23(1), 015607 (2012).
43. S. Kumaraguru, J. Yesuraj, and S. Mohan, Reduced graphene oxide-wrapped micro-rod like Ni/Co organic–inorganic hybrid nanocomposite as an electrode material for high-performance supercapacitor. *Compos. Part B Eng.* 185, 107767 (2020).
44. Y. Liu, Y. He, E. Vargun, T. Plachy, P. Saha, and Q. Cheng, 3D porous Ti<sub>3</sub>C<sub>2</sub> MXene/NiCo-MOF composites for enhanced lithium storage. *Nanomaterials* 10(4), 1–14 (2020).
45. P. Thangasamy, S. Shanmuganathan, and V. Subramanian, A NiCo-MOF nanosheet array based electrocatalyst for the oxygen evolution reaction. *Nanoscale Adv.* 2(5), 2073–2079 (2020).
46. Y. Chi, W. Yang, Y. Xing, Y. Li, H. Pang, and Q. Xu, Ni/Co bimetallic organic framework nanosheet assemblies for high-performance electrochemical energy storage. *Nanoscale* 12(19), 10685–10692 (2020).
47. Y.P. Zhu, Y.L. Liu, T.Z. Ren, and Z.Y. Yuan, Hollow manganese phosphonate microspheres with hierarchical porosity for efficient adsorption and separation. *Nanoscale* 6(12), 6627–6636 (2014).
48. C. Qu, Y. Jiao, B. Zhao, D. Chen, R. Zou, K.S. Walton, and M. Liu, Nickel-based pillared MOFs for high-performance supercapacitors: design, synthesis and stability study. *Nano Energy* 26, 66–73 (2016).
49. B. L. Xiang, L. Fu, Y. Li, and Y. Liu, Preparation of Fe(II)/MOF-5 catalyst for highly selective catalytic hydroxylation of phenol by equivalent loading at room temperature. *J. Chem.*, 2019 (2019).
50. B. Zhang, S. Song, W. Li, L. Zheng, and X. Ma, Asymmetric supercapacitors with high energy density and high specific capacitance based on Ni-Co-Mn multiphase metal structure MOF. *Ionics (Kiel)* 27(8), 3553–3566 (2021).
51. Z. Jin-Da, L. Li-Bing, and Y. Ze-Qing, High energy density supercapacitor electrode materials based on mixed metal MOF and its derived C@bimetal hydroxide embedded onto porous support. *Synth. Met.* 277, 116775 (2021).
52. S. Gao, Y. Sui, F. Wei, J. Qi, Q. Meng, Y. Ren, and Y. He, Dandelion-like nickel/cobalt metal–organic framework based electrode materials for high performance supercapacitors. *J. Colloid Interface Sci.* 531, 83–90 (2018).
53. J. Sun, X. Yu, S. Zhao, H. Chen, K. Tao, and L. Han, Solvent-controlled morphology of amino-functionalized bimetal metal–organic frameworks for asymmetric supercapacitors. *Inorg. Chem.* 59(16), 11385–11395 (2020).
54. G. Zhu, H. Wen, M. Ma, W. Wang, L. Yang, L. Wang, X. Shi, X. Cheng, X. Sun, and Y. Yao, A self-supported hierarchical Co-MOF as a supercapacitor electrode with ultrahigh areal capacitance and excellent rate performance. *Chem. Commun.* 54(74), 10499–10502 (2018).
55. Y. Liang, W. Yao, J. Duan, M. Chu, S. Sun, and X. Li, Nickel cobalt bimetallic metal–organic frameworks with a layer-and-channel structure for high-performance supercapacitors. *J. Energy Stor.* 33, 2020 (2021).
56. P.A. Shinde, Y. Seo, S. Lee, H. Kim, Q.N. Pham, Y. Won, and S.C. Jun, Layered manganese metal–organic framework with high specific and areal capacitance for hybrid supercapacitors. *Chem. Eng. J.* 387, 122982 (2020).
57. C.R. Mariappan, V. Gajraj, S. Gade, A. Kumar, S. Dsoke, S. Indris, H. Ehrenberg, G.V. Prakash, and R. Jose, Synthesis and electrochemical properties of rGO/polypyrrole/ferrites nanocomposites obtained via a hydrothermal route for hybrid aqueous supercapacitors. *J. Electroanal. Chem.* 845, 72–83 (2019).
58. M. Isacfranklin, R. Yuvakkumar, G. Ravi, S.I. Hong, F. Shini, M. Thambidurai, C. Dang, and D. Velauthapillai, Marigold flower like structured Cu<sub>2</sub>NiSnS<sub>4</sub> electrode for high energy asymmetric solid state supercapacitors. *Sci. Rep.* 10(1), 1–12 (2020).

**Publisher's Note** Springer Nature remains neutral with regard to jurisdictional claims in published maps and institutional affiliations.

Springer Nature or its licensor (e.g. a society or other partner) holds exclusive rights to this article under a publishing agreement with the author(s) or other rightsholder(s); author self-archiving of the accepted manuscript version of this article is solely governed by the terms of such publishing agreement and applicable law.

## Authors and Affiliations

Amruta D. Salunkhe<sup>1,2</sup>  · P. K. Pagare<sup>1</sup> · A. P. Torane<sup>1,2</sup>

✉ A. P. Torane  
appasahebtorane@yahoo.in

Amruta D. Salunkhe  
amrutasalunkhe38@gmail.com

<sup>1</sup> Solid State Physics Laboratory, Department of Physics, Yashwantrao Chavan Institute of Science (Autonomous), Satara 415001, India

<sup>2</sup> Rayat Institute of Research Development Center, Satara 415001, India